

Analogue benchmarks of shortening and extension experiments

GUIDO SCHREURS¹, SUSANNE J. H. BUITER², DAVID BOUTELIER³,
GIACOMO CORTI⁴, ELISABETTA COSTA⁵, ALEXANDER CRUDEN³,
JEAN-MARC DANIEL⁶, SILVAN HOTH⁷, HEMIN KOYI⁸, NINA KUKOWSKI⁷,
JO LOHRMANN⁷, ANTONIO RAVAGLIA⁹, ROY W. SCHLISCHE¹⁰,
MARTHA OLIVER WITHJACK¹⁰, YASUHIRO YAMADA¹¹, CRISTIAN CAVOZZI⁵,
CHIARA DELVENTISETTE¹², JENNIFER A. ELDER BRADY¹⁰,
ARNE HOFFMANN-ROTHER⁷, JEAN-MARIE MENGUS⁶,
DOMENICO MONTANARI¹² & FARAMARZ NILFOROUSHAN⁸

¹*Institute of Geological Sciences, University of Bern, Baltzerstrasse 1-3, CH-3012 Bern, Switzerland (e-mail: schreurs@geo.unibe.ch)*

²*Centre for Geodynamics, Geological Survey of Norway, 7491 Trondheim, Norway*

³*Department of Geology, University of Toronto, 22 Russell St., Toronto, Ontario M5S 3B1, Canada*

⁴*CNR-Istituto di Geoscienze e Georisorse, Sezione di Firenze, via G. La Pira 4, I-50121 Firenze, Italy*

⁵*Dipartimento di Scienze della Terra, Università di Parma, Parco Area delle Scienze 157/A, I-43100 Parma, Italy*

⁶*Institut Français du Pétrole, 1 et 4 avenue de Bois Préau, F-92500 Reuil Malmaison, France*

⁷*GeoForschungsZentrum Potsdam, Telegrafenberg, D-14473 Potsdam, Germany*

⁸*Hans Ramberg Tectonic Laboratory, Department of Earth Sciences, Uppsala University, Villavägen 16, S-75326 Uppsala, Sweden*

⁹*Dipartimento di Scienze della Terra, Università di Pavia, via Ferrata 1, I-27100 Pavia, Italy*

¹⁰*Department of Geological Sciences, Rutgers University, Piscataway, NJ, 08854, USA*

¹¹*Department of Civil and Earth Resources Engineering, Kyoto University, Kyoto 606-5801 Japan*

¹²*Dipartimento di Scienze della Terra, Università di Firenze, via G. LaPira 4, 1, I-50121 Firenze, Italy*

Abstract: We report a direct comparison of scaled analogue experiments to test the reproducibility of model results among ten different experimental modelling laboratories. We present results for two experiments: a brittle thrust wedge experiment and a brittle-viscous extension experiment. The experimental set-up, the model construction technique, the viscous material and the base and wall properties were prescribed. However, each laboratory used its own frictional analogue material and experimental apparatus. Comparison of results for the shortening experiment highlights large differences in model evolution that may have resulted from (1) differences in boundary conditions (indenter or basal-pull models), (2) differences in model widths, (3) location of observation (for example, sidewall versus centre of model), (4) material properties, (5) base and sidewall frictional properties, and (6) differences in set-up technique of individual experimenters. Six laboratories carried out the shortening experiment with a mobile wall. The overall evolution of their models is broadly similar, with the development of a thrust wedge characterized by forward thrust propagation and by back thrusting. However, significant variations are observed in spacing between thrusts, their dip angles, number of forward thrusts and back thrusts, and surface slopes. The structural evolution of the brittle-viscous extension experiments is similar to a high degree. Faulting initiates in the brittle layers above the viscous layer in close vicinity to the basal velocity discontinuity. Measurements of fault dip angles and

fault spacing vary among laboratories. Comparison of experimental results indicates an encouraging overall agreement in model evolution, but also highlights important variations in the geometry and evolution of the resulting structures that may be induced by differences in modelling materials, model dimensions, experimental set-ups and observation location.

Geoscientists have used scaled experimental models (from here on also referred to as analogue models) for more than a century to gain insight into the kinematic and dynamic evolution of geological structures (e.g., Cadell 1888; Ramberg 1981; Koyi 1997). The ability to observe structures while they form is both attractive and insightful, and the ease with which model experiments can be performed has certainly contributed to their widespread application. Although many experiments have investigated similar geological processes, a direct comparison of experiments using the same prescribed set-up has until now been lacking. Testing the reproducibility of model results among different laboratories is important as it allows for documentation of the degree to which variations in model apparatus, modelling materials and experimental techniques can affect the outcome of experiments. Assessing the reliability of analogue models also has implications for comparisons between structures formed in experimental models, results of numerical simulations and natural field examples.

We present the results of two analogue ‘benchmarks’: a shortening experiment and an extension experiment. Ten modelling laboratories participated in these experiments. The experimental set-up, the construction technique, the viscous material (employed in the extension experiment) and the material covering walls and base were prescribed. Since each laboratory used its own frictional analogue material (sand, microbeads, wet clay) and experimental apparatus, our study is not a benchmark in its strictest sense. Our aims are to (1) indicate the degree of reproducibility of model results between different laboratories, (2) highlight the influence of material properties, model boundary conditions and experimental set-up, and (3) use our results to suggest further benchmark experiments.

The two experimental set-ups were designed to simulate upper-crustal processes, and can be placed among a wide range of laboratory experiments studying contractional and extensional deformation. Numerous studies document experiments of thrust wedges under normal gravity conditions (e.g., Davis *et al.* 1983; Malavieille 1984; Mulugeta & Koyi 1987, 1992; Mulugeta 1988; Colletta *et al.* 1991; Lallemand *et al.* 1994; Koyi 1995; Storti & McClay 1995;

Mugnier *et al.* 1997; Gutscher *et al.* 1996, 1998; Storti *et al.* 2000; Schreurs *et al.* 2001; Turrini *et al.* 2001; Kukowski *et al.* 2002; Costa *et al.* 2004; Hoth *et al.* 2005). Deformation in these experiments occurs either by displacing a back wall or by pulling a basal sheet below a fixed wall. Such indenter-type or basal-pull-type models are not entirely equivalent, as we will discuss below. Parameters investigated in published thrust wedge experiments include basal friction, the presence of décollement layers, dip of the initial basal surface, surface slope, and the effects of erosion. In general, such models display a series of forward-propagating, in-sequence thrusts, whereby changes in, for example, basal friction or erosion may cause renewed hinterland activity. Many authors have investigated brittle-viscous extension in a normal gravity field (e.g., Tron & Brun 1991; Vendeville & Jackson 1992*a, b*; Brun *et al.* 1994; Keep & McClay 1997; Brun 1999; Gartrell 2001; Bahroudi *et al.* 2003). In these models, a viscous layer typically overlies a velocity discontinuity at the base of the model and is itself overlain by brittle materials. In all experiments the viscous basal layer exerts a strong control on fault nucleation and location.

In a companion paper, Buitter *et al.* (2006) present numerical equivalents of both analogue experiments and compare the results qualitatively and quantitatively. This study shows that numerical models employing different techniques (finite-element, finite-difference and distinct element methods) are able to reproduce results of analogue models successfully. The combination of analogue and numerical modelling methods may help establish the robust features of models of crustal-scale processes (e.g., Ellis *et al.* 2004; Pysklywec & Cruden 2004; Panien *et al.* 2006).

Methods

Material properties

We focus on experiments performed in a natural gravity field. In such experiments dry sand or wet clay are commonly used to simulate brittle rocks in the upper crust, and viscous materials to simulate salt or lower crustal rocks. In the shortening experiment, the models consisted of granular

materials (sand and glass microbeads) only, whereas for the extension experiment both brittle and viscous materials were used. All laboratories used the same polydimethylsiloxane (PDMS) as viscous material. This is a linear viscous material (silicone polymer) with a viscosity of 5×10^4 Pas at room temperature and at strain rates below $3 \times 10^{-3} \text{ s}^{-1}$ (Weijermars 1986; see also Ten Grotenhuis *et al.* 2002; Cruden *et al.* 2006). In contrast, each laboratory used its own brittle materials, which generally differed in density, frictional properties, grain sizes and grain shape (Table 1). Several laboratories measured the frictional properties of their granular materials using either a Hubbert-type shear box (Hubbert 1951), a ring-shear tester (Schulze 1994) or a Casagrande shear box (Casagrande 1932). Errors in ring-shear measurements are usually small (less than 1%). Measurements in Hubbert-type shear boxes are less precise, because of the larger uncertainty associated with the determination of the exact timing of the onset of shearing. As the Casagrande shear box measurements in this study employed higher normal loads than occur in the experiments, the measured values for cohesion are not considered representative for the experimental conditions.

Although experimental modellers have often assumed that their brittle materials deform according to the Coulomb failure criterion with constant frictional properties, several studies demonstrate that materials such as quartz sand, corundum sand and glass microbeads are characterized by elastic/frictional plastic behaviour with strain-hardening preceding failure (at peak strength) and subsequent strain-softening until a stable value is reached (Lohrmann *et al.* 2003; Panien 2004). Such mechanical behaviour is very similar to the one exhibited by experimentally deformed rocks (e.g., Jaeger & Cook 1979; Marone 1998; Barnhoorn *et al.* 2004). Values for the angle of internal friction (at peak strength) range from 33° to 45° for quartz sand and from 21° to 29° for microbeads (Table 1). These values are generally comparable to those determined experimentally for upper crustal rocks (Byerlee 1978). Strain-softening may be expressed as the percentage difference between peak friction and dynamic stable friction. For the materials used in this study, it varied from 4% to 20% for quartz sand and from 0% to 14% for microbeads (Table 1). In each case, strain softening in microbeads was lower than in sand. Cohesion values of granular materials display a wide range varying between -25 and 150 Pa. The negative values and the large variation in cohesion values may be related to

uncertainties in the linear extrapolation of the failure envelope to very low normal stresses. At low normal stresses, the failure envelope is no longer a straight line, but has a convex-leftward shape with negligible cohesion (Schellart 2000). One laboratory (Piscataway) used wet clay instead of dry sand for the extension experiment. Their clay has an elasto-plastic rheology with an angle of peak friction of 27° .

To reduce the influence of the variable properties of sidewalls and base of the modelling apparatus, they were covered with a self-adhesive, transparent PVC foil (brand Alkor, article number 120010). The influence of this foil was investigated by measuring the friction between sand and the foil in the GFZ ring-shear tester. **Q1.1** For fine-grained sand ($20\text{--}200 \mu\text{m}$) the angle of peak friction was $19.8^\circ \pm 0.1^\circ$ and the angle of stable friction was $16.5^\circ \pm 0.3^\circ$. For coarser-grained sand ($20\text{--}650 \mu\text{m}$) the angles of peak and stable friction were $19.7^\circ \pm 0.1^\circ$ and $16.7^\circ \pm 0.3^\circ$, respectively. This implies that the use of different sands in the experiments probably had only little influence on values of boundary friction, as long as Alkor foil was used on all sidewalls and the base.

Differences in frictional properties of the model materials may be attributed to the applied measuring technique (e.g., Casagrande shear box, Hubbert-type shear box or ring-shear tester), the filling technique and/or intrinsic material properties such as grain size distribution, grain shape and composition (Table 1). Variations in material properties may be important for differences in the evolution of experimental models. Lohrmann *et al.* (2003) found that the kinematics of thrust wedges are largely a function of their material properties. Adam *et al.* (2005) point out that the strength increase of the granular materials during the strain-hardening phase towards peak strength influences the localization and early development of faults. A detailed investigation of the exact causes of the differences in material properties is beyond the scope of our study, but it should be kept in mind that our modelling results are influenced by the use of different granular materials.

Scaling

Our models aim at representing upper-crustal conditions and can be scaled up to natural dimensions by observing geometric, kinematic and dynamic similarity relationships (Hubbert 1937; Ramberg 1981). We assume that 1 cm in the models corresponds to 1 km in nature and that (dimensionless) angles of internal friction can

Table 1. Material properties and grain characteristics

Laboratory	Density (kg m^{-3})	C at ϕ_{peak} (Pa)	ϕ_{peak} ($^{\circ}$)	ϕ_{stable} ($^{\circ}$)	Strain soft. (%)	Grain size (μm)	Grain shape	Composition
<i>Bern</i>								
Quartz sand*	1560	21 ± 18	35.5	31.2	15	80–200	angular	99% SiO ₂
Conundum sand*	1890	39 ± 10	37	32.2	16	88–125	angular	95% Al ₂ O ₃
Microbeads*	1480	25 ± 4	22.3	20.6	8	70–110	well-rounded	72.5% SiO ₂ 13.8% Na ₂ O 8% CaO
<i>Florence</i>								
Quartz sand	1550	66	39	n.d.	n.d.	<250	rounded	n.d.
<i>Kyoto</i>								
Quartz sand	1390	n.d.	n.d.	34	9	m = 203	angular	93% SiO ₂ 4% Al ₂ O ₃
Microbeads	1420	n.d.	n.d.	25	0	m = 193	spherical	Na ₂ O–CaO–SiO ₂
<i>Parma</i>								
Quartz sand [†]	1500	†	34.1	n.d.	n.d.	60–250	Sub-rounded	99.8% SiO ₂
Microbeads	1540	n.d.	n.d.	n.d.	n.d.	m = 180	rounded	n.d.
<i>Pavia</i>								
Quartz sand [†]	1500	†	33.2	32.1	4.1	60–250	angular to sub-angular	99.8% SiO ₂
Microbeads [†]	1550–1600	†	26.4	26.2	1	150–250	well-rounded	n.d.
<i>Piscataway</i>								
Clay [‡]	1600	~40	27	n.d.	n.d.	<100	platy	Kaolinite + 40–50% H ₂ O
<i>GFZ Potsdam</i>								
Quartz sand*	1740	94 ± 7	35.4 ± 0.3	28.2 ± 0.05	20.2	20–630 (m = 350)	well-rounded	95% SiO ₂
Microbeads*	1590	-6 ± 19	29.1 ± 0.14	22.5 ± 0.04	13.6	300–400	well-rounded	n.d.

<i>IFF Rueil-Malmaison</i>										
Quartz sand	1500	n.d.	45	39	19	m = 116	angular	>98% SiO ₂		
Corundum sand	1880	n.d.	39	34	16.7	m = 108	angular	>98% Al ₂ O ₃		
Microbeads	1400–1600	n.d.	n.d.	n.d.	n.d.	m = 121	well-rounded	72.5% SiO ₂ 13.8% Na ₂ O 8% CaO		
<i>Toronto</i>										
Quartz sand*	1625	3	35.7	29.2	22.2	150–200	angular	>98% SiO ₂		
Microbeads*	1575	41	25.5	23.4	9.2	~100	rounded	n.d.		
<i>Uppsala</i>										
Quartz sand [§]	1350	~150	33	30	11	60–250	angular	97% SiO ₂		
Microbeads [§]	1440	~50	21	20	5	m = 125 53–105	rounded	73 % SiO ₂ 12.5% Na ₂ O 8.5% CaO 4.5% MgO		

C = cohesion; m = median of grain size; ϕ_{peak} = angle of peak friction; ϕ_{stable} = angle of stable-dynamic friction; strain-softening is measured as the difference between coefficient of peak friction and coefficient of stable-dynamic friction divided by the coefficient of peak friction. n.d. = not determined.

* Angles of peak friction, stable-dynamic friction and inferred cohesion determined with a ring-shear tester (Schulze 1994) at GFZ Potsdam.

† Angles of peak friction and stable-dynamic friction determined with a Casagrande shear box (Casagrande 1932) at high normal loads; these normal loads are much higher than those in the experiments. Values of cohesion obtained by linear regression of high normal stress Casagrande tests are questionable (Pavia: ~ 686 Pa for microbeads, and 21378 Pa for sand; Parma: 12000 Pa for sand).

‡ Angle of peak internal friction and inferred cohesion determined with a ring-shear tester (Sims 1993).

§ Angles of peak friction, stable-dynamic friction and inferred cohesion determined with a Hubbert-type shear box (Hubbert 1951) at low normal loads comparable to those produced in analogue experiments presented here.

be taken to be equal at both scales. Then,

$$\frac{C_p}{\rho_p} = 10^5 \frac{C_m}{\rho_m} \quad (1)$$

where subscript p denotes natural conditions, subscript m analogue model conditions, C is cohesion and ρ is density. Using representative densities ρ_m c. 1600 kg m^{-3} and ρ_p c. 2800 kg m^{-3} , a cohesion of 10 Pa in the model corresponds to around 2 MPa in nature. The scaling up of viscous properties depends on the assumed velocity v (v_m was prescribed in our experiments):

$$\frac{\eta_p v_p}{\rho_p} = 10^{10} \frac{\eta_m v_m}{\rho_m} \quad (2)$$

for viscosity η .

Shortening experiment

Model set-up

In the shortening experiment a thrust wedge was built in alternating layers of different strength. Six laboratories (Bern, Parma, Pavia, IFP Rueil-Malmaison, Toronto, Uppsala) deformed their model by moving the backwall (right-hand wall in our figures) of the apparatus towards the interior of the model (leftward). For ease of description these models are referred to as mobile back wall models (Fig. 1a). Two laboratories (Kyoto and GFZ Potsdam) produced shortening by pulling an underlying sheet horizontally beneath the vertical backwall. These models are referred to as fixed back wall models (Fig. 1b). The applied shortening rate varied between the models. This was not expected to influence the results as only rate-independent brittle model materials were used.

The model dimensions (length and width) varied between the laboratories (Table 2). The mechanical stratigraphy was the same in all models. A 5 mm thick layer of sand at the base of the apparatus was overlain by a 5 mm thick layer of weaker microbeads, which in turn was overlain by additional layers of sand (Fig. 1a, b). To visualize deformation, the sand layers above the microbeads were either coloured differently or alternated with corundum sand, which has similar mechanical properties to quartz sand (laboratories of Bern and IFP Rueil-Malmaison, Table 1). The total thickness of the layers was 3.5 cm. The granular materials were sieved from a height of 20 cm with a filling rate of approximately 250 grams/minute. The model was not pre-compacted before the onset

of shortening. A wedge of sand, 10 cm long and with a 10° surface slope was sieved adjacent to the right-hand vertical wall to facilitate the build up of the thrust wedge. The base of the modelling apparatus remained horizontal.

As the Alkor foil created visualization problems across glass sidewalls, the laboratories of Kyoto, Parma and Pavia did not apply foil on the sidewalls, while GFZ Potsdam applied the foil only on the sidewall which was not used for visualization. Two laboratories (Kyoto and Parma) tested the sensitivity of the experimental results to the presence of Alkor foil on the sidewalls. For most laboratories no significant material loss through a gap at the base of the right-hand vertical wall was reported. In the two fixed back wall experiments (Kyoto and GFZ Potsdam) there was a small exit slot (<1 mm) above the conveyor belt. In the Toronto experiment, there was initially no slot below the right-hand mobile wall, but at the end of the experiment a small slot (<1 mm) appeared.

All laboratories monitored the cross-sectional evolution, either by photography through transparent sidewalls (GFZ Potsdam, Kyoto, Parma, Pavia, Toronto and initial stage of Uppsala) or by X-ray CT imaging through the centre of the model (Bern and IFP Rueil Malmaison) (Table 2). The laboratory from Uppsala monitored mainly the surface evolution of the model and cut a cross-section through the central part of the model at the end of the experiment.

Comparison of mobile back wall model results

Figure 2 shows the cross-sectional structural evolution of the eight thrust wedge models after 0, 2, 6, 10 and 14 cm of displacement. A comparison of surface structures of three of the models (Fig. 3) shows a difference in drag of the structures along the sidewalls (walls parallel to the shortening direction). Thrusts are convex to the hinterland for the fixed back wall models and convex to the foreland for the mobile back wall models. Because the two shortening setups led to differences in structural evolution and given that the majority of the experiments were mobile back wall models, we only compared quantitative parameters related to the cross-sectional geometry for the six mobile back wall models.

To compare model results quantitatively, we measured the following parameters for up to 14 cm of displacement (Table 3, Figs 4 and 5): the amount of displacement at which forward thrusts form (Fig. 4a), their basal and upper dip

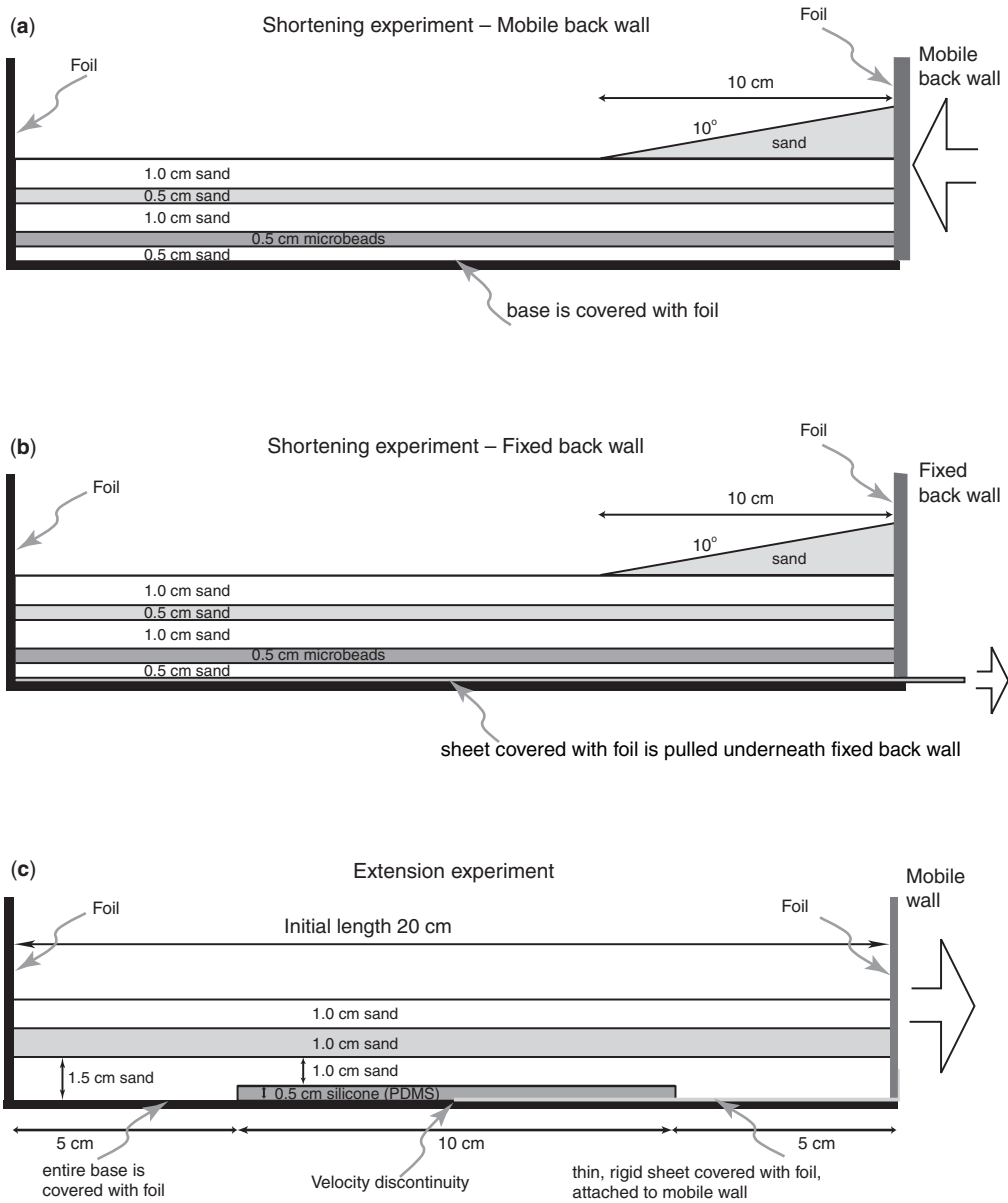


Fig. 1. (a) Setup of the shortening experiment with a mobile back wall. The mobile back wall moves leftward (towards the foreland). (b) Setup of the shortening experiment with a fixed back wall. Shortening is achieved by pulling a basal sheet below the fixed wall. (c) Setup of the extension experiment. A thin viscous slab of PDMS, 10 cm wide and 5 mm high, lies in the central part of the model. Half of the PDMS overlies the thin rigid sheet that is attached to the mobile wall. The mobile wall moves rightward.

angle (Figs 4b and c, respectively; see Fig. 4 for definition), the dip angle of back thrusts (Fig. 4d), the spacing between forward thrusts (measured as the distance to the previous thrust at the moment of initiation of a new thrust) (Fig. 4e), the surface slope of the wedge

(Fig. 5), the amount of fault-controlled shortening, the displacement at which the microbeads layer was activated and the length of the detachment in the microbeads layer (Table 3). The amount of shortening accommodated by faults is determined from the offset of

Table 2. *Model dimensions and details of model set-up*

Laboratory	Model dimensions* (cm) (shortening experiment)	Model dimensions* (cm) (extension experiment)	Fixed or mobile back wall (shortening experiment)	Alkor foil sidewalls parallel to displ. direction	Small exit slot (shortening experiment)	Thickness rigid basal sheet (extension experiment)	Monitoring method	Other changes with respect to prescribed set-up
Bern	35.8 × 80	20 × 80	Mobile	Yes	No	0.5 mm	CT scan	
Florence [†]	n.a.	20 × 90	n.a.	Yes	n.a.	?	Surface, final sections	
Kyoto	94 × 50	20 × 25	Fixed	No	0.5 mm	n.a.	Surface, side	
Parma [‡]	60 × 33	n.a.	Mobile	Yes	No	n.a.	Surface, side, final sections	
Pavia	60 × 33	n.a.	Mobile	No	No	n.a.	Surface, side	
Piscataway	70 × 30	n.a.	Mobile	No	No	n.a.	Surface, side	
	n.a.	20 × 61	n.a.	No	n.a.	0.2 mm	Surface, final sections	Extension to 3 cm
GFZ Potsdam	340 × 20	n.a.	Fixed	No	1 mm	0.3 mm	Surface, side	
IFP Rueil-Malmaison	37 × 78	20 × 78	Mobile	Yes	No	0.5 mm	CT scan	
Toronto	41.9 × 45	29.2 × 45	Mobile	Yes	Late stage, < 1 mm [§]	1.6 mm	Surface, side (short), final sections	Initial width ext. expt. 29.2 cm
Uppsala	41 × 30	n.a.	Mobile	Yes	No	n.a.	Surface, final sections	

*Dimensions of model (length × width); length is measured parallel and width perpendicular to shortening or extension direction.

[†]Two extensional experiments were performed with different model widths.

[‡]Two shortening experiments were performed with and without Alkor foil on the sidewalls (see Fig. 4 for results with Alkor foil).

[§]A small exit slot (< 1 mm) formed at the end of the experiment as the piston-wall was slightly uplifted.

n.a. = not applicable.

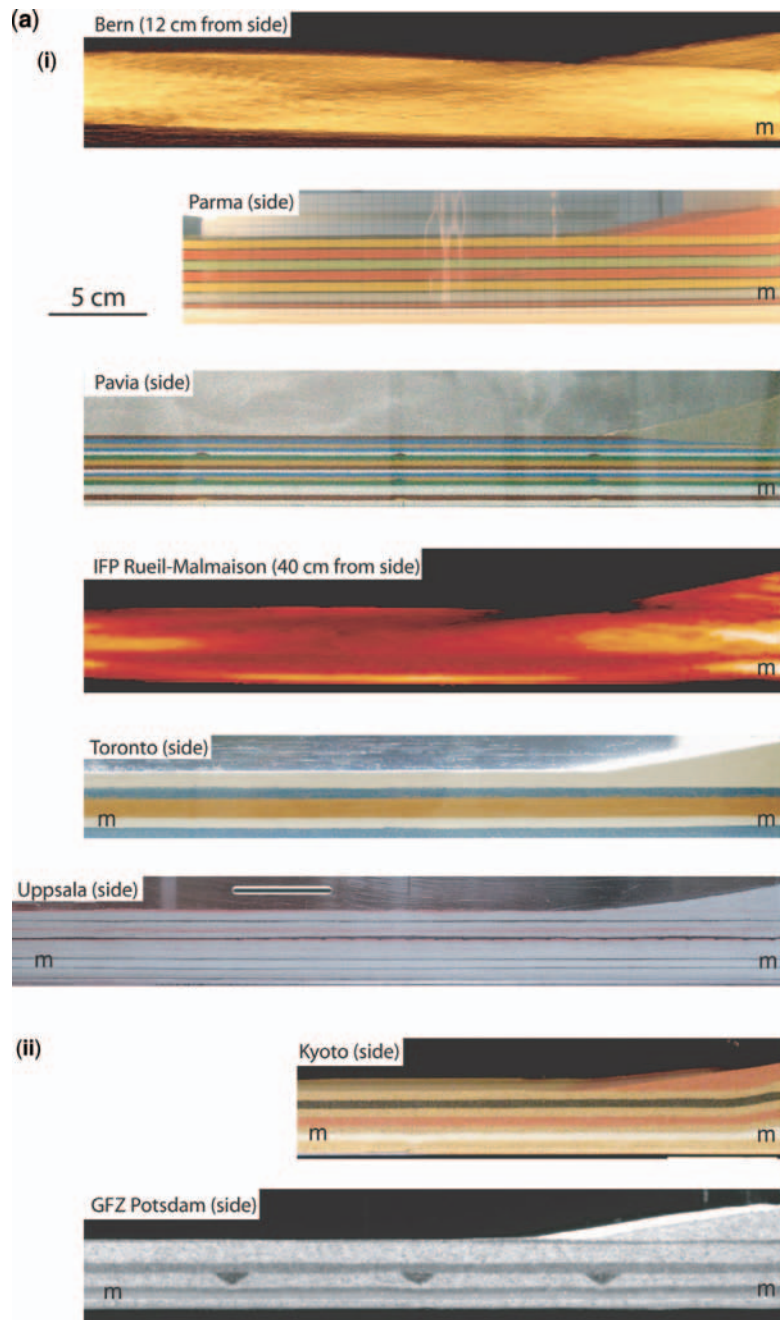


Fig. 2. Results for the shortening experiments for mobile back wall (i) and fixed back wall (ii) models. The microbeads layer is indicated by an 'm'. Model length is not shown completely for all laboratories (see also Table 2). Note slightly oblique views for the Toronto model. The microbeads layer is not well visible in CT images of the early stages of the Bern and IFP Rueil-Malmaison experiments. **(a)** Initial geometries. The locations of the cross-sections are indicated with the laboratory names. **(b)** Geometries after 2 cm displacement. **(c)** Geometries after 6 cm displacement. **(d)** Geometries after 10 cm displacement. **(e)** Geometries after 14 cm displacement. The Uppsala model has been covered with an additional sand layer before cutting of section.

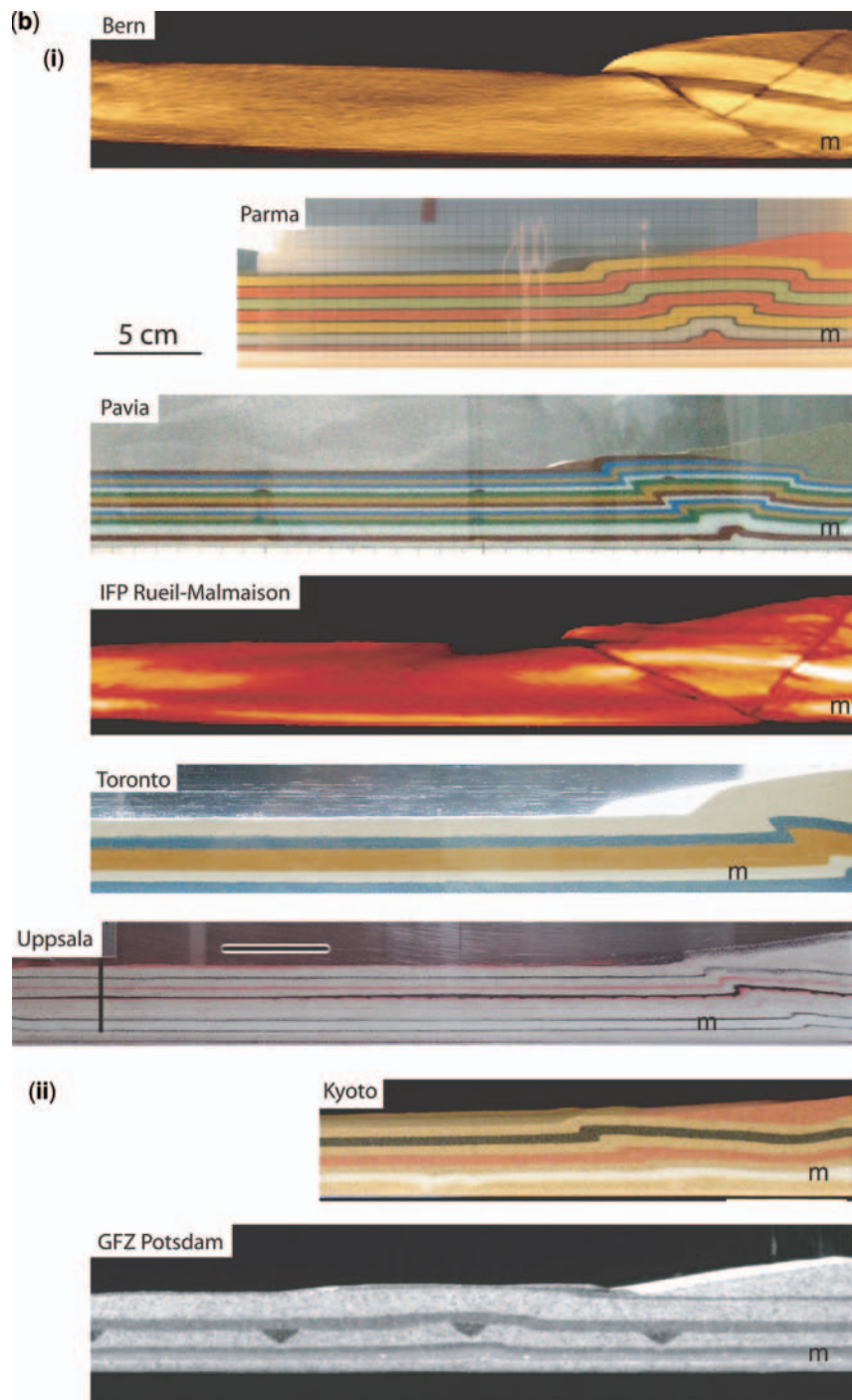


Fig. 2. *Continued.*

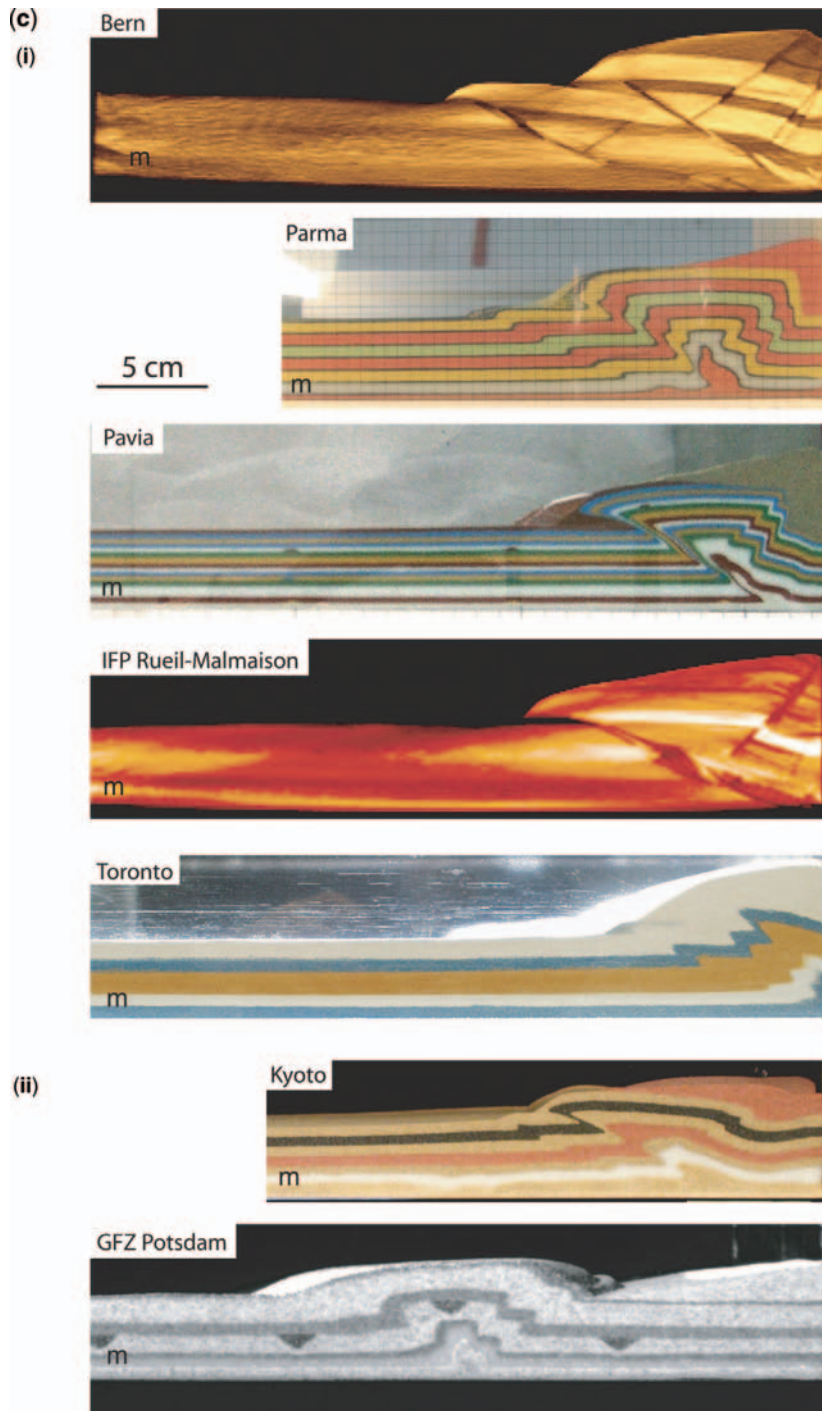


Fig. 2. Continued.

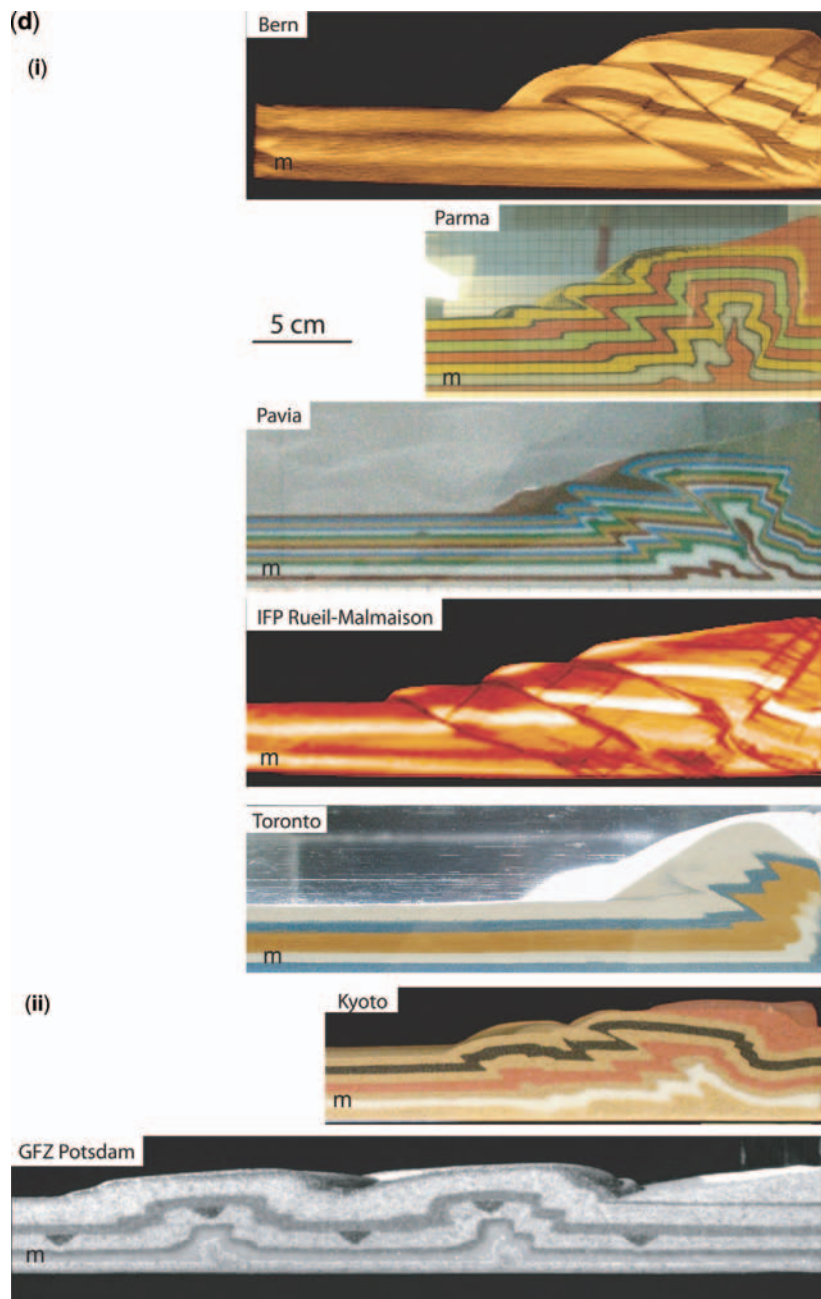


Fig. 2. *Continued.*

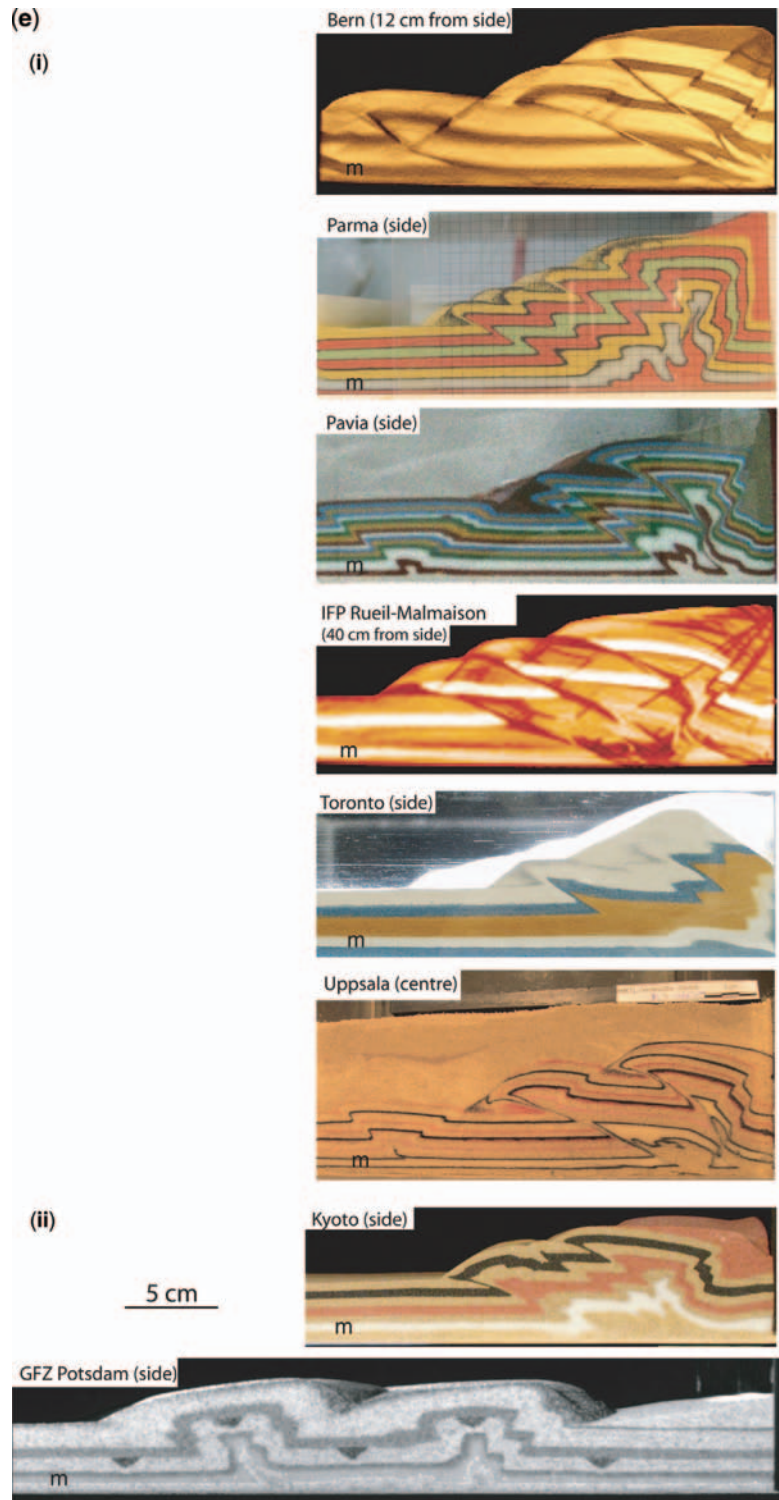


Fig. 2. Continued.

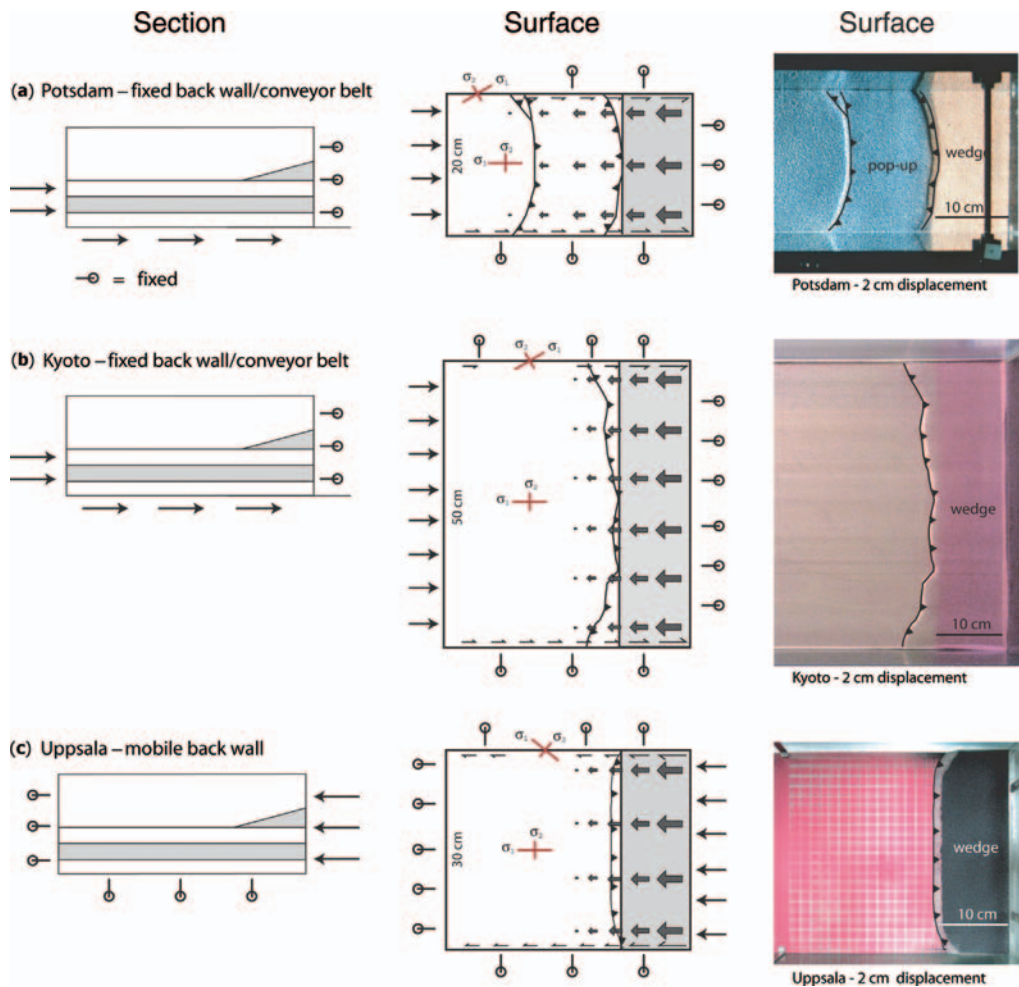


Fig. 3. Left-hand column: Cross sections of fixed and mobile back wall model set-ups. Middle column: Surface views with sense and relative magnitude of horizontal shear stresses acting at the base of the model (filled arrows) and shear stresses acting at depth along the lateral sidewalls (half arrows). The rotation of σ_1 from pure compression in the centre of the model to strike-slip at the sides explains the sense of curvature of the surface traces of the reverse faults. Right-hand column: Surface views of models after 2 cm displacement. (a) Fixed back wall model of Potsdam (model width 20 cm). (b) Fixed back wall model of Kyoto (model width 50 cm). (c) Mobile back wall model of Uppsala. Note the difference in drag of structures along the sidewalls between fixed and mobile back wall models. Grey-shaded area in column in the middle indicates the initial location of the sand wedge.

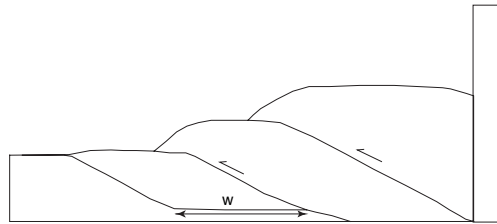
WebColor

cut-off points of material layers by the faults. Quantitative analysis used sections along the lateral boundaries (Parma, Pavia and Toronto, initial stage of Uppsala) or through the centre of the model using X-ray CT images (Bern, IFP Rueil-Malmaison). Analysis of the Uppsala model was mainly done by monitoring the surface evolution and by cutting a section through the model at the end of deformation. Thus we could not measure all parameters for this experiment. As in the equivalent numerical

models (Buiter *et al.* 2006), we found that the measurements were sensitive to the person measuring due to small differences in interpretation. Therefore, two people measured parameters for all experiments (using cross-sectional images taken at 1 cm increments of displacement) in the same manner and averaged the obtained values. In general the differences between the two measurers were small, with a maximum variation in fault dip angle values of 6° .

Table 3. Quantification of mobile back wall shortening experiments

Laboratory	Fault shortening* at 4 cm (cm)	Microbeads layer	
		Activated at (cm)	Detachment length (cm)
Bern	2.85	5	6.6
Parma	n.d. [†]	11	2.2
Pavia	1.9	no	–
IFP Rueil- Malmaison	2.75	no [‡]	–
Toronto	1.9	10.8	9.3
Uppsala	n.d.	12.3	12.7



*Fault-controlled horizontal shortening determined by cut-off points between layers and the faults.

[†]In the model of Parma fault-controlled shortening was not determined as the faults are not narrow shear zones, but rather wide kink-like structures with deflection of layers towards the kink zones.

[‡]Reactivation of microbeads with a detachment length of 1.8 cm occurred along strike at 9 cm shortening.

Inset at bottom shows how detachment length (w) was measured.

The mobile back wall models share the following similarities: (1) Shortening is accommodated by forward thrusts, which propagate in-sequence towards the foreland, and by back thrusts (Fig. 2). (2) After 2 cm of displacement, an active forward thrust formed in all models (Fig. 2b). (3) The dip angles of this first forward thrust are fairly similar: $28^\circ \pm 4^\circ$ for its lower dip and $29^\circ \pm 3^\circ$ for its upper dip. Upper dip angles are generally slightly steeper (Figs 4b and c). (4) The dip angle of back thrusts is higher than the dip angle of forward thrusts (Fig. 4d).

From Figures 2, 4 and 5 and Table 3 it is also clear that variations in thrust wedge deformation occur among the models: (1) The number of forward thrusts that formed at a particular amount of displacement is variable (maximum difference of two thrusts) (Figs 2 and 4a). (2) Five experiments show the first thrust propagating upward from a point located to the left of the base of the back wall, whereas two experiments (Toronto, Fig. 2b and one model of Parma, Fig. 6a, b) show the forward thrust propagating from the corner at the base of the back wall. The reason for this difference is not entirely clear. A comparison of mobile back wall models whose

evolution was monitored through glass sidewalls suggests that the presence of Alkor foil along the sidewalls could promote the formation of forward thrusts emanating from the lower right-hand corner. Cross-sections cut after 14 cm displacement located near or adjacent to the transparent sidewalls are shown in Figure 6 for the two models that applied Alkor foil to the sidewalls (one model of Parma and Toronto). In both models a large number of forward thrusts formed very close to the mobile wall. The absence of back thrusts close to the mobile wall for these models is in agreement with the formation of forward thrusts rooting at the basal right-hand corner, as this does not leave space for the formation of back thrusts propagating from the base. Alternatively, the variation in first thrust configuration could be caused by variation in sand properties. Shear zones may be located close to the mobile wall for sand in which peak strength is reached fast. Variations in friction along the back wall or in the height of the gap below the right-hand wall (however small) may also play a role.

(3) Four experiments (Bern, Parma, Pavia, IFP Rueil-Malmaison) show the formation of a back

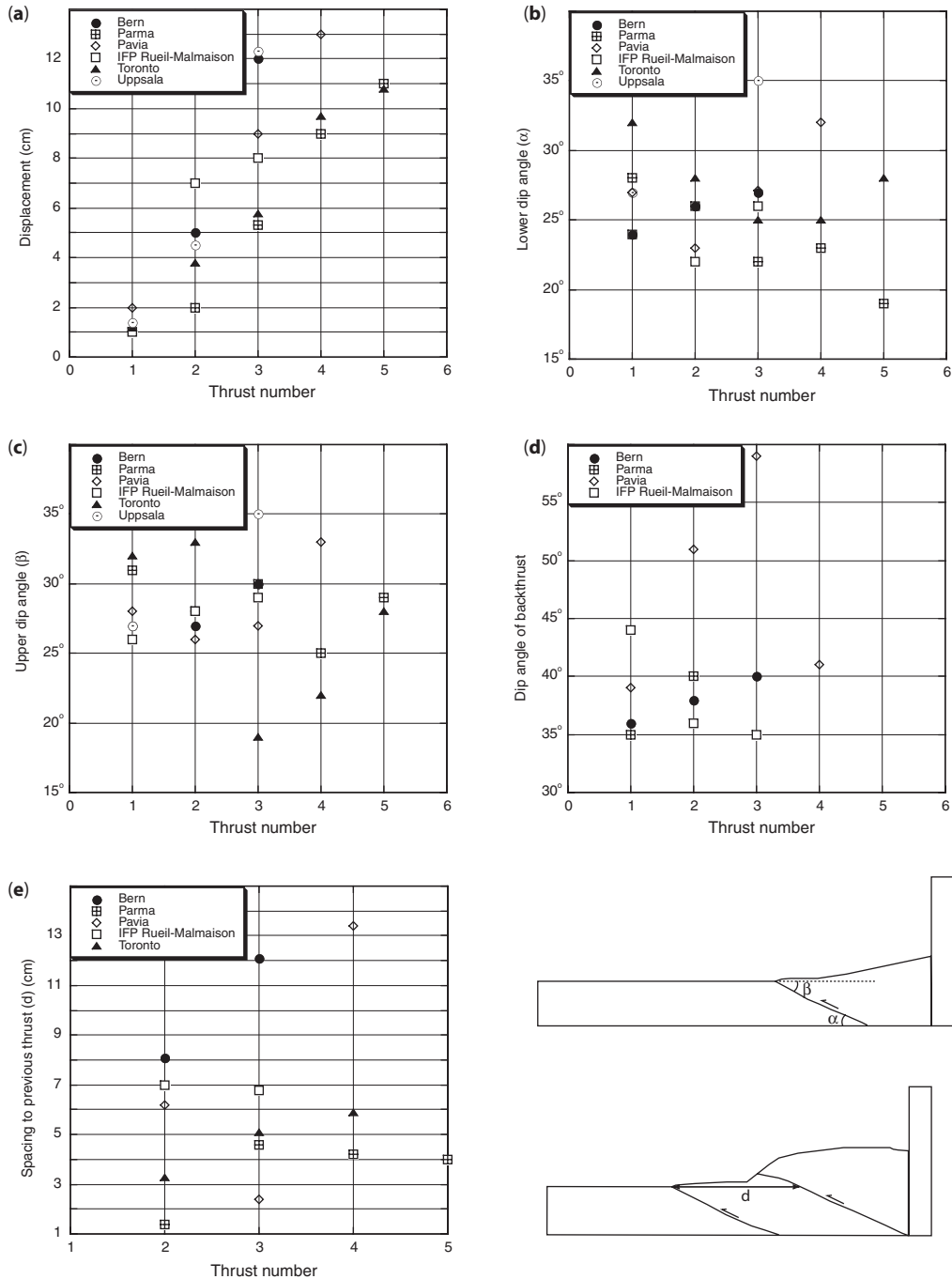


Fig. 4. Quantitative comparison of the six mobile back wall models. All values were measured at the moment a new fault initiated. (a) The amount of displacement at which a forward thrust forms. (b) Lower dip angle of forward thrusts. (c) Upper dip angle of forward thrusts. (d) Dip angle of back thrusts. (e) Spacing to previously formed forward thrust at the moment of initiation of a new forward thrust. Insets at right-hand lower corner show how lower dip angle (α), upper dip angle (β) and thrust spacing (d) were measured.

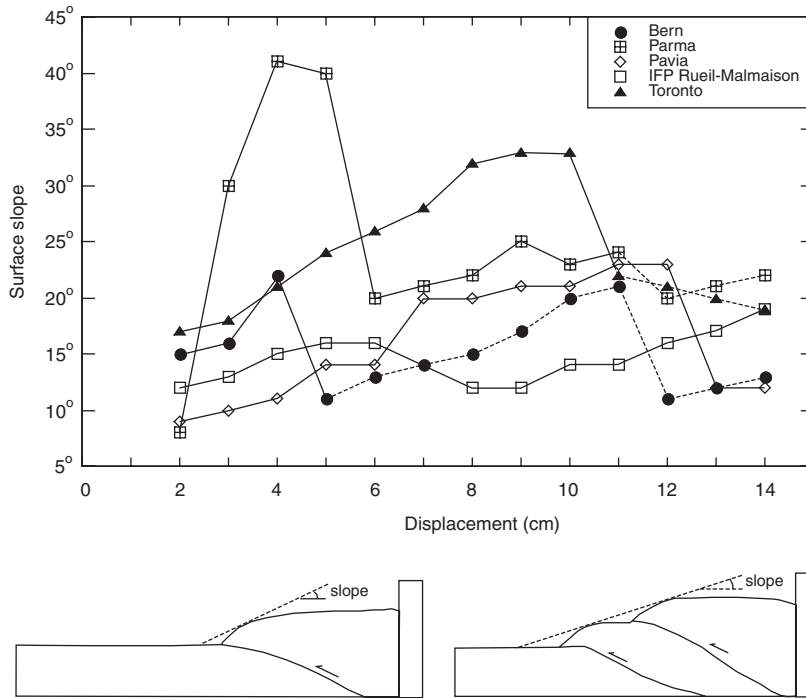


Fig. 5. Surface slope versus displacement for five mobile back wall models. Lines are solid when the microbeads layer has not been activated and dotted after activation of the microbeads layer. The insets show how surface slope was measured for one thrust (left) and for more than one thrust (right).

thrust related to the first thrust. In three of these experiments, the back thrust roots onto the base of the model and connects with the upper right-hand corner of the wedge. In the Bern experiment, however, the first back thrust roots at the top of the microbeads layer and does not connect with the upper right-hand corner of the wedge. In this experiment, CT images reveal that the back thrust forms later than the forward thrust. The back thrust rooting at the top of the microbeads layer suggests sensitivity to small variations in material properties (between sand and microbeads) for the Bern model (Fig. 2). In the Toronto experiment back thrusts did not form until 12 cm of displacement and are then related to the frontal thrust (Fig. 6f). (4) The distance between a newly formed thrust and the previously formed thrust is highly variable (Fig. 4e). (5) The microbeads layer was activated in four experiments (Bern, Parma, Toronto, Uppsala). In one experiment (IFP Rueil-Malmaison) activation of microbeads occurred along strike of the sections shown in Figure 2, based on CT scans. In the Pavia experiment, no activation took place (Table 3). (6) The length of the

detachment in the microbeads layer is variable (Table 3).

(7) The surface slope of the wedge is also highly variable (Fig. 5). The high surface slope angles at 3 to 5 cm of displacement in the Parma experiment are the result of a second forward thrust that formed very close to the first one (with a thrust spacing of only slightly over 1 cm; Fig. 4e). Oscillations in surface slope angles occur as new thrusts form. The thrust wedges do not seem to reach a stable state. It may be that more displacement is needed before a stable field is reached (Lohrmann *et al.* 2003). Alternatively, alternating use of the embedded microbeads layer or the base of the model for forward thrust propagation may disturb stable surface slopes. The strength contrast between the microbeads layer and the base may be comparable, depending on the sand and microbeads used. Figure 6 shows no clear effect on surface slope of the first activation of the embedded microbeads layer. (8) Fault-controlled shortening at 4 cm of displacement varies between 48 and 71%, implying that diffuse deformation and deformation taken up by folding ranges from 29 to 52%.

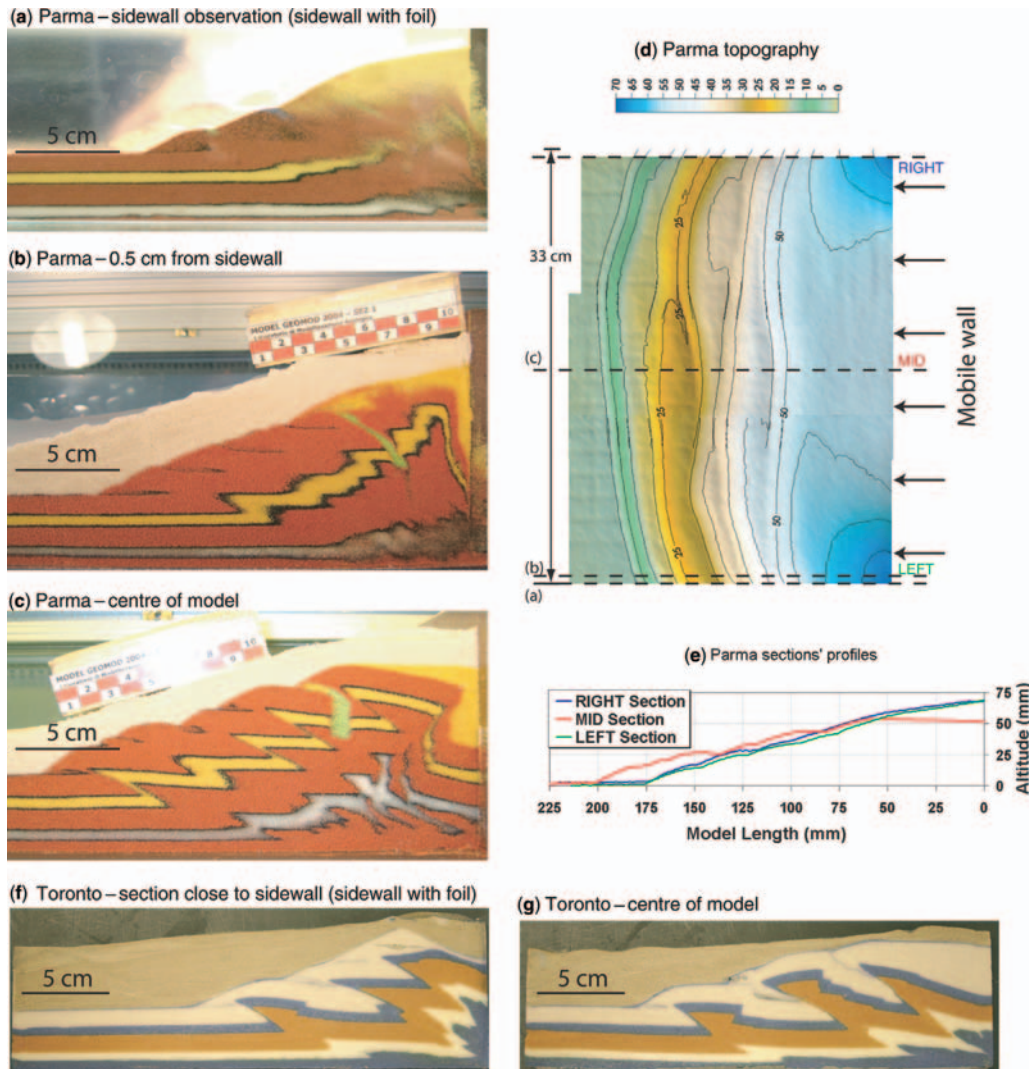


Fig. 6. Influence of lateral shear stresses illustrated in models of Parma (a–e) and Toronto (f and g). Structures are shown after 14 cm displacement. This model of Parma shown is with Alkor foil attached to the sidewalls (and is, therefore, different from the model in Fig. 2). The model of Toronto also has Alkor foil applied to the sidewalls (same model as in Fig. 2). (a) Cross section as observed through glass sidewalls. Note that Alkor foil partly obscures model visualization. (b) Cross section at 0.5 cm from sidewall. (c) Cross section through centre of model. (d) Contour map showing topography of deformed model, obtained by laser scanner; scale in cm above model base. (e) Topographic profiles 0.5 cm from sidewalls (right and left section) and through centre of model ('mid section'). (f) Cross section close to lateral sidewall. (g) Cross section through centre of model. Note that in (b), (c), (f) and (g) a sand layer was added on top of the model before cutting.

WebColor

Effects of experimental set-up, material properties and boundary conditions

The geometry and evolution of the structures in the shortening experiments reflects differences in experimental set-up, material properties and model dimensions.

The surface structures in Figure 3 show that thrusts are convex to the hinterland for fixed back wall models and convex to the foreland for mobile back wall models. Although the absolute magnitude of the basal and lateral shear stresses are not known, the curved geometry along the

sidewalls indicates differences in stress trajectories between fixed and mobile back wall models. The sense and relative magnitude of the basal shear stresses at the onset of shortening are the same for both fixed and mobile back wall models. The basal shear stresses are highest near the back wall and decrease away from it as a result of both decreasing wedge load and increasing distance from the back wall. The sense of the lateral shear stresses, however, is different for the fixed and mobile back wall models. The lateral shear stresses in the fixed back wall models are directed towards the fixed back wall, i.e., in a direction opposite to the basal shear stresses. In contrast, in the mobile back wall models the direction of the lateral shear stresses is the same as that of the basal shear stresses. The difference in sense of lateral shear stresses for fixed and mobile back wall models results in the difference in drag of structures near the sidewalls (compare Figs 3a and b with Fig. 3c). In both cases, the drag is in the same direction as the sense of the lateral shear stresses and can be understood from the rotation of the σ_1 (most compressive stress) direction from pure compression in the centre of the models towards strike-slip at the sides (Fig. 3).

In the fixed back wall model of Potsdam, a pop-up structure formed in front of the pre-existing wedge with the back thrust close to its toe (Figs 2b and 3a). The pre-existing wedge itself was not involved in the thrusting. The initial localization of deformation in front of the wedge in the Potsdam experiment (20 cm width) is similar to other fixed back wall model experiments with an initial wedge geometry and comparable initial thicknesses (Gutscher *et al.* 1996, 1998 (30 cm width); Konstantinovskaia & Malavieille 2005 (10 cm width)). In the mobile back wall models, a forward thrust or box fold structure forms close to the mobile wall and deforms the pre-existing wedge (Figs 2 and 3c). The fixed back wall model of Kyoto (Figs 2 and 3b) shows a structural evolution that is more similar to the mobile back wall models, with a forward thrust surfacing close to the toe of the wedge. A main difference between the Potsdam and Kyoto fixed back wall models is the width (measured perpendicular to shortening direction): the Potsdam model is 20 cm wide and 340 cm long, and the Kyoto model is 50 cm wide and 94 cm long. This suggests that model width has an important influence on the overall structural evolution of the thrust wedge. Comparisons of the Kyoto and Potsdam models (Figs 3a and b) suggest that the effect of lateral shear stresses on model structures is more

important in narrow models. The width of a model apparatus needs careful attention, therefore, balancing between minimization of edge effects which occur in narrow models and minimization of heterogeneities due to, for example, hand sieving, which tends to be amplified in wide models.

The set-up of our shortening experiment required that at least 14 cm inward displacement could be accommodated without deformation reaching the back wall. Activation of the microbeads layer may cause thrusting to step further out than for a homogeneous sand layer, and a longer initial domain length will consequently be needed in that case. The region in front of the foremost thrust may, depending on the type of sand used, strain-harden upon shortening, and deformation of the wedge may be influenced if the strain-hardening front reaches the back wall. Adam *et al.* (2005) show that the region of diffuse strain accumulation in front of the wedge can have a length of approximately 15 cm (for a 3.5 cm high input layer). Some models in our study may in their late deformation stages have been affected by the length of the model apparatus, as deformation and/or the region of strain-hardening has reached the back wall. The length of the model apparatus should, therefore, also be considered carefully when designing an experiment.

The effects of lateral shear stresses on the shape of the thrust wedge during shortening are illustrated in Figure 6 for two mobile back wall models (Parma and Toronto). The cross-sectional wedge geometries at different locations (Figs 6a–c and 6f–g), the final model topography (Fig. 6d) and topographic profiles along different cross-sections (Fig. 6e) show that the thrust wedge shortens and steepens toward the sidewalls due to the shear stresses along the sidewalls. It is important, therefore, to evaluate the along-strike (perpendicular to the shortening direction) variation of model results. The effects of sidewall properties on model evolution could be tested by repeating the same experiment while varying only the materials of the walls.

As the properties of the granular materials varied significantly, it was not to be expected that all experiments would develop in an identical manner. The set-up of our comparison is, furthermore, not suitable to uniquely distinguish the effects of the differences in material properties from the influence of other variables such as model boundary conditions and dimensions. This can be tested by performing the same experiment in the same apparatus with different granular materials (Lohrmann *et al.* 2003).

Implications of the shortening experiments

The shortening experiments show that differences in material properties, boundary conditions (fixed back wall versus mobile back wall models) and model dimensions may result in significant differences in model results. Despite these differences, a comparison of the mobile back wall models demonstrates similar styles of deformation in which shortening is accommodated by both in-sequence forward propagation of thrusts and, in most models, by back thrusts. We consider this an encouraging result, which will help establish robust features in laboratory tectonic models. The variations in geometry and structural evolution among the mobile back wall models may be attributed to (1) differences in properties of the granular materials, (2) small variations in the exit slot below the mobile wall, (3) differences in the location of observation (at sidewall versus centre of model), (4) the properties of the walls (presence or absence of Alkor foil), (5) width of the box (due to influence of lateral shear stresses), (6) length of the model (for short domain lengths), and (7) set-up technique (for example, small variations may occur when sieving granular layers by hand and levelling of layers after sieving may lead to some compaction).

Our results indicate that care has to be taken when evaluating quantitative results from model experiments and applying them to natural systems. This is especially the case when results are obtained from measurements through transparent sidewalls (where lateral shear stresses are greatest). Although analogue models may be qualitatively used to interpret the mechanics of thrust wedges, limitations apply to quantifiable results such as thrust spacing, surface slope, length of detachment layer and the number of thrusts versus shortening.

Extension experiment

Model set-up

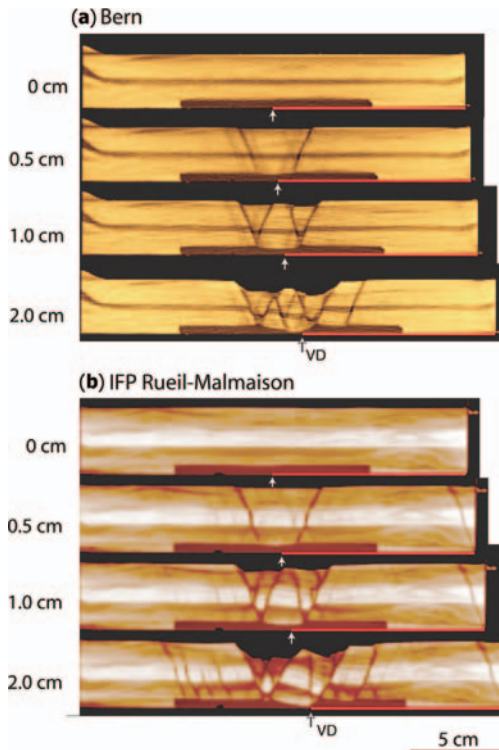
The extension experiment tested the influence of a weak, basal viscous layer on fault localization in overlying brittle materials (Fig. 1c). Five modelling laboratories ran the extension experiment (Bern, Florence, Piscataway, IFP Rueil-Malmaison and Toronto). The initial length (measured parallel to the extension direction) was 20 cm in all models, except for Toronto, where it was 29.2 cm. The width of the model, measured perpendicular to the extension direction, was variable (Table 2). The Florence laboratory ran two experiments with

different widths (25 and 90 cm). Alkor foil covered the base and sidewalls of the experimental apparatus. A thin sheet, also covered with Alkor foil, lay on the base of the apparatus. It extended from the centre of the apparatus to a mobile end wall (right-hand side in all figures) and was attached to it. Extension was produced by moving the mobile wall with the attached sheet outward at a constant velocity of 2.5 cm/hour. The edge of the mobile sheet acted as a velocity discontinuity. Total displacement was 5 cm, except for the Piscataway model where it was 3 cm.

A 10 cm long and 5 mm thick slab of viscous PDMS covered the central part of the apparatus. To minimize PDMS sticking to the sidewalls, Vaseline was applied over a height of 5 mm from the right end (mobile) wall to the left end of the PDMS layer. Four models used dry sand and one model (from Piscataway) used wet clay as the brittle analogue material (Table 1). Sand was sieved (from a height of 20 cm with a filling rate of approximately 250 grams/minute) or clay was placed adjacent to and on top of the basal PDMS slab. Multiple sand (or clay) layers had the same material properties (as much as possible), but different colours to help in visualizing deformation. The model was not pre-compacted before the onset of extension. The total height of the model was 3.5 cm. No sedimentation occurred during extension. Two laboratories (Bern and IFP Rueil-Malmaison) monitored the model cross-sectional evolution by X-ray CT imaging through the centre of the model and three laboratories (Florence, Toronto, Piscataway) by monitoring the surface evolution and by cutting a cross-section through the centre after the end of the experiment.

Model results

Figure 7 shows the cross-sectional evolution of the models Bern and IFP Rueil-Malmaison for four stages of displacement (0, 0.5, 1 and 2 cm). Figure 8 illustrates the final cross-sectional geometry of all five models. Surface views at 2 cm displacement are shown in Figure 9. We measured the following parameters for a quantitative comparison of the models: the amount of displacement at which the first faults formed and their fault dip angle (Table 4), the amount of fault-controlled extension (Table 4), the displacement at which faults formed at the edges of the silicone layer (Table 4), and the dip angle and migration of the first-formed normal fault to the right of the velocity discontinuity with increasing extension (Fig. 10). Due to different monitoring procedures not all



WebColor **Fig. 7.** Cross-sectional geometries of two extension experiments at 0, 0.5, 1 and 2 cm displacement. The horizontal red line indicates the position of basal thin sheet covered with Alkor foil. The tip of the basal sheet is indicated with a white arrow (VD = velocity discontinuity). (a) Model of Bern. The cross-section is taken 35 cm from the side (see Fig. 9). (b) Model of IFP Rueil-Malmaison. The cross-section is taken through the centre of the model.

parameters could be determined for all laboratories. The values were again measured by two people and then averaged.

Analysis of the qualitative and quantitative aspects of the experimental model results allows the following observations:

(1) After 1 cm of displacement, fault zones are visible in all models. In most models, faults formed near the centre of the model and with additional extension, the faulted zone broadened, with younger faults propagating towards the edges of the silicone layer (Fig. 7). In the narrow model of Florence (25 cm width), the model evolution differed (Fig. 9). The first faults nucleated onto the right-hand edge of the silicone layer and much of the subsequent extension was accommodated along these faults. In this narrow experiment, the velocity discontinuity had no influence on localizing initial

deformation. With additional extension, most faulting concentrated in the brittle layers along the right-hand edge of the silicone layer and only minor faulting occurred in the centre and left-hand side of the model. In two other models (Toronto and Florence large-width model), early faulting also nucleated at the right-hand edge of the silicone, but nearly simultaneously with the development of faults near the central velocity discontinuity. Faulting in the central part of the model subsequently accommodated most of the continued extension. All sand-silicone models demonstrate that the rheological change between the viscous silicone layer and the brittle sand cover, combined with friction along the sidewalls, may result in the nucleation of faults along the edges of the silicone layer.

(2) All models show drag structures due to friction along the sidewalls (Fig. 9). The sense of the curvature of the surface views of the normal faults can be understood from the rotation of σ_3 (least compressive stress) from pure extension in the centre of the model towards strike-slip at the sides (see also Vendeville 1987).

(3) The first formed faults have dip angles of 60° to 69° in sand layers and dip angles of 55° to 58° in clay. These dip angles correspond closely to those expected for Mohr-Coulomb faults, for which the fault dip should be $45^\circ + \phi/2$ (Coulomb angle).

(4) The cross-sectional evolution of the Bern and IFP Rueil-Malmaison models, obtained by X-ray CT imaging through the centre of the model, shares many similarities. Extension first leads to the formation of two main fault in the central part of the model on either side of the velocity discontinuity (Fig. 7; panels at 0.5 cm). These faults are initially symmetrically located with respect to the velocity discontinuity. However, the fault extrapolations do not root directly above the velocity discontinuity, but are offset laterally. This may be explained by more distributed thinning of the silicone layer, which smooths out the influence of the velocity discontinuity. Further displacement along the two main normal fault causes further thinning and sideways expulsion of the silicone layer and results in the formation of two conjugate fault sets (Fig. 7; panels at 1 cm). As displacement of the basal sheet continues, the initial symmetry of the first deformation structures is disrupted. The silicone continues to thin, the surface depression becomes wider and asymmetric in shape, and the faulted zone broadens outward.

(5) The dip angle of the first formed normal fault on the right side of the velocity discontinuity that dips away from the mobile wall decreases with continued extension (Fig. 10a). For larger amounts of displacement (5 cm), faults tend to

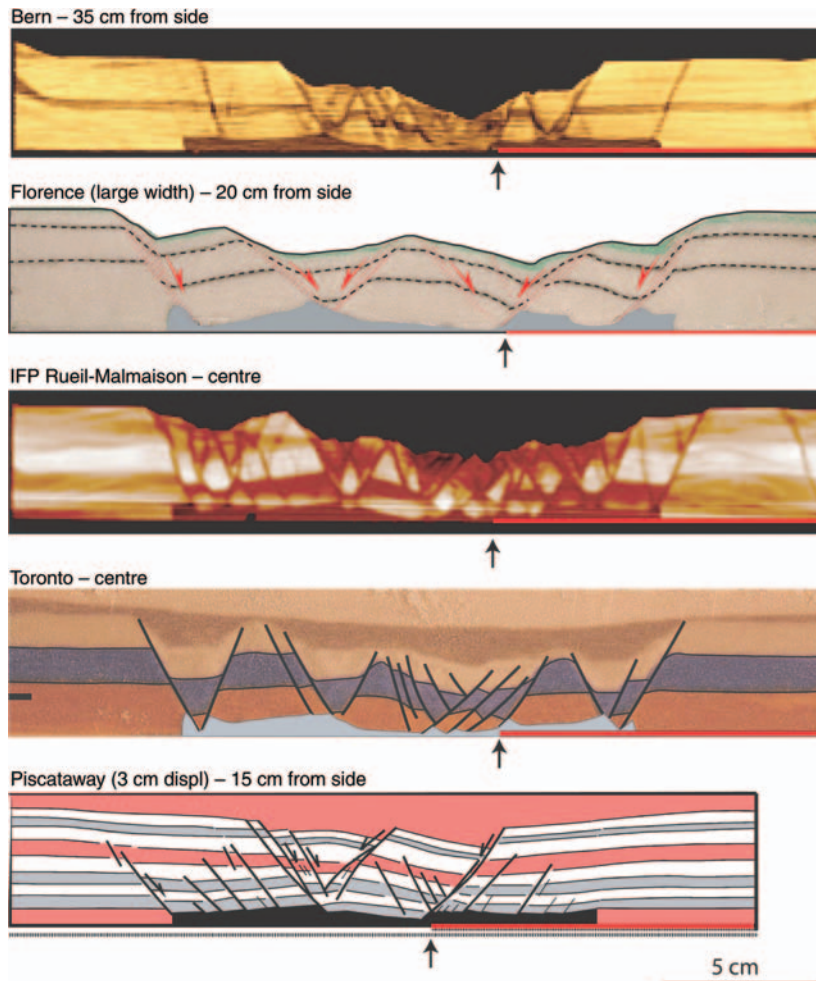


Fig. 8. Cross-sectional geometries at 5 cm displacement for the extension models of Bern, Florence (model of 90 cm width), IFP Rueil-Malmaison and Toronto. The Piscataway clay model is at 3 cm displacement (line-drawing after photograph). A sand layer has been added to the models of Toronto and Piscataway before cutting. The horizontal red line indicates the position of the basal thin sheet covered with Alkor foil. The tip of the basal sheet (the velocity discontinuity) is indicated with a small arrow.

WebColor

become listric and block rotations become more pronounced.

(6) The first-formed normal fault on the right side of the velocity discontinuity (dipping away from the right end wall) moves to the right as the model is extended (Fig. 10b). In the models of Bern and IFP Rueil-Malmaison fault migration is similar and in both cases slower than the displacement velocity of the mobile wall because continued extensional deformation is also accommodated by the formation of new faults in the block located to the right of the first formed normal fault.

(7) The amount of fault-controlled extension at 2 cm could be measured in three experiments and ranges between 0.8 cm in the silicone-clay model and 0.9 to 0.95 in the silicone-sand models.

Implications of the extension experiments

As in the shortening experiment, we find that the width of the model (perpendicular to the extension direction) may cause differences in model results. Lateral friction seems to have a larger influence on initial fault location and evolution

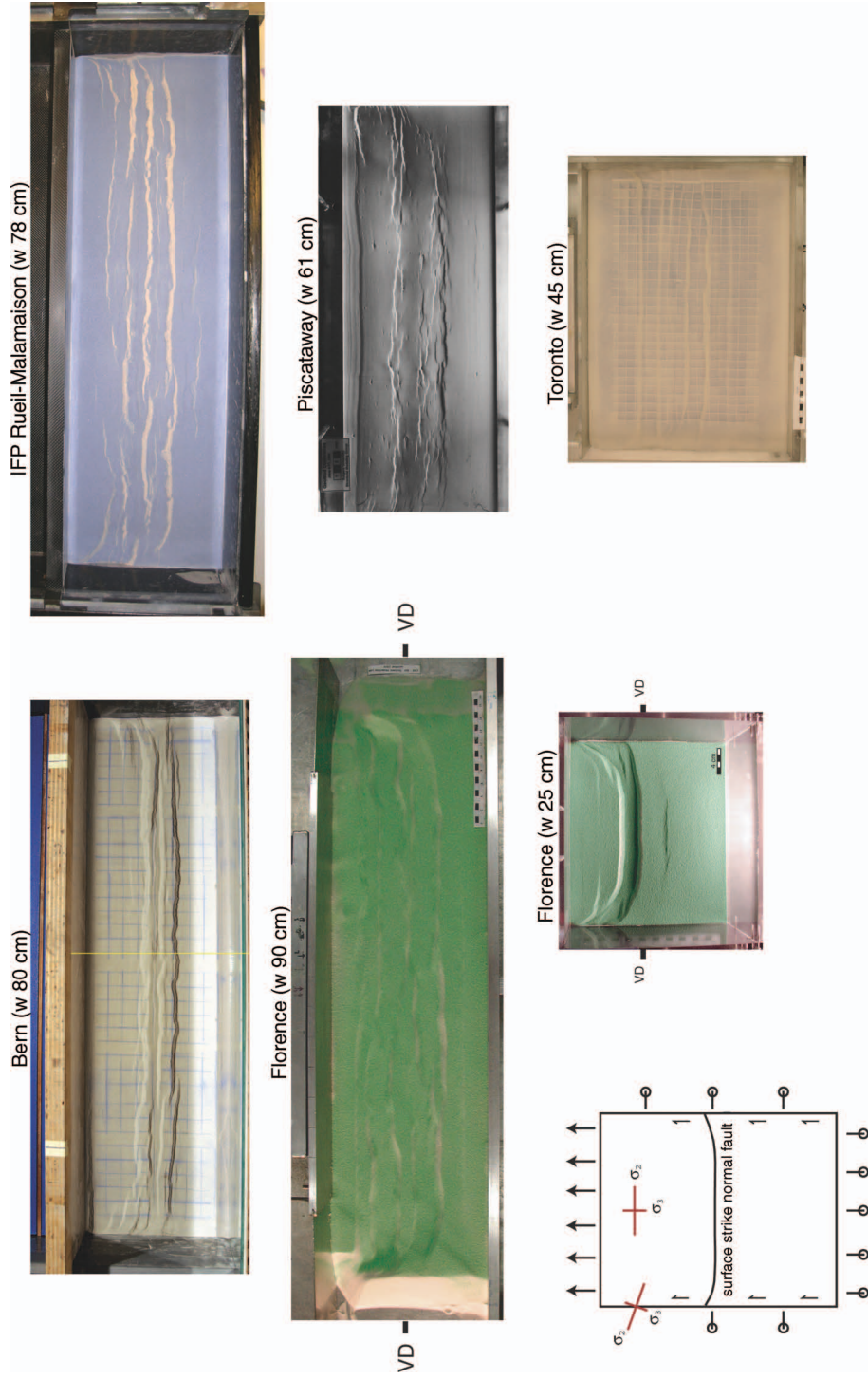


Fig. 9. Surface views of the extension models of Bern, Florence (25 cm and 90 cm wide models), IFP Rueil-Malmaison, Piscataway (57 cm of 61 cm width is shown) and Toronto at 2 cm displacement. The width of the models is indicated with the laboratory names at the top of each panel. The mobile wall is at the top of each panel. Inset shows how the rotation of σ_3 from pure extension in the middle of the model to strike-slip at the sides explains the direction of the drag structures at the sidewalls.

Table 4. *Quantification of extension experiment*

Laboratory	Fault extension* at 2 cm (in cm)	Fault initiation at edges of PDMS (at cm of extension)		First fault on left side of VD dipping toward mobile wall		First fault on right side of VD dipping away from mobile wall	
		Left	Right	Dip angle	At extension (cm)	Dip angle	At extension (cm)
Bern	0.9	never	4–4.5	69°	<0.5	65°	<0.5
Florence†	n.d.	1	1	60°‡	<0.5	§	
Piscataway	0.8	2	never	55°‡		58°‡	
IFP Rueil-Malmaison	0.95	never	2–2.5	65°	<0.5	60°	<0.5
Toronto	n.d.	1.2	0.6	62°	0.6–1.2	62°	0.6–1.2

*Fault-controlled horizontal extension determined by cut-off points between layers and the faults.

†Results shown are for large-width (90 cm) model.

‡Fault dip measured at surface.

§First two faults that form both dip towards mobile wall.

|| Fault dip measured at surface; faults dip shallower towards bottom of model.

VD = velocity discontinuity.

Q1.4

in narrow models than in the wider models. A comparison between the Toronto model (29.2 cm length) and the other models (20 cm length) (Fig. 8) shows no clear indication for influence of the length of the model for this set-up. In wide models the main graben forms initially above the velocity discontinuity, as observed in the equivalent numerical models (Buiter *et al.* 2006). A comparison between these models shows a high level of agreement with respect to initial fault dip and graben location, graben broadening and decrease in fault dip with continued extension. However,

variability in structural evolution does occur and includes differences in the number of normal faults that form and the timing with which faulting propagates to the edges of the viscous layer. The differences in evolution between the models may be attributed to (1) differences in material properties, (2) differences in model width, (3) possible small variations of initial silicone slab geometry, (4) variations in base and wall properties, and (5) differences in location of observation. Similar to the shortening experiment, our results indicate that caution is required when quantitative results such as the

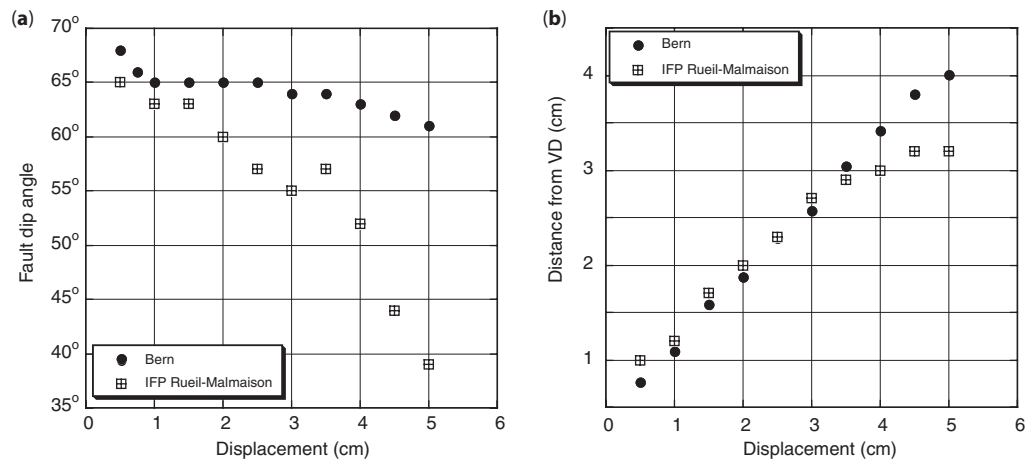


Fig. 10. (a) Dip angle versus displacement for the first formed normal fault on the right side of the velocity discontinuity and dipping away from the mobile wall. (b) Normal fault migration in the extension experiment. The migration of the first formed normal fault on the right side of the velocity discontinuity and dipping away from the mobile wall is measured relative to the velocity discontinuity (VD).

number and spacing of faults are extrapolated from analogue models to natural systems.

Conclusions and outlook

We used two experimental set-ups to test the reproducibility of model results among different experimental modelling laboratories. We find that all models demonstrate a similar first order evolution. The differences among the models in our study may help to identify main focus points for future comparison studies.

A comparison of eight brittle thrust-wedge experiments shows that model evolution may differ in detail to a considerable extent. These differences may be related to: (1) differences in model set-up (i.e., two laboratories used a conveyor belt below a fixed back wall and six laboratories used a mobile back wall above a fixed horizontal base), (2) differences in model dimensions, (3) location of observation (i.e., at the transparent sidewall or in the centre of the model), (4) material properties of granular materials (angle of internal friction, cohesion and amount of strain softening and strain hardening), (5) mechanical properties along the walls (with or without Alkor foil), (6) small differences in the set-up technique used by individual experimenters ('the human factor'). All mobile back wall experiments show the development of a thrust wedge characterized by in-sequence forward thrusts and minor back thrusting. A large variability exists in quantitative parameters such as fault dip, thrust spacing, number of forward and back thrusts, and surface slope.

The evolution of wide extension models is highly similar. Normal faulting initiates in the brittle layers above the viscous silicone layer, near the basal velocity discontinuity. Fault dip angles tend to shallow with continued extension. Variations between laboratories occur for parameters such as fault dip angle and fault spacing. Reducing the variability in quantifiable parameters such as number of faults and fault spacing will be a challenge for future analogue benchmarks.

The present study is the first ever comparison of analogue experiments between different modelling laboratories and our results may be used as a guide for the design of future comparison studies. Future 'benchmarks' could focus on: (1) a simpler experimental design to minimize the number of differences in experimental set-up among the participating laboratories, (2) use of the same materials in comparison studies between different laboratories (to test the influence of model apparatus and experimenter), (3) measuring the properties of a sample of the same material in different shear testers in order

to determine the influence of the measuring method, (4) additional tests of the influence of material properties for different materials and experimental set-ups (where the same experimenter repeats the same experiment in the same laboratory and modelling apparatus), following up on previous studies (e.g., Lohrmann *et al.* 2003; Atmaoui *et al.* 2005; Withjack & Callaway 2000), (5) having different experimenters perform the same experiment using one apparatus (in the same laboratory) to test the 'human factor', (6) testing the variability of quantifiable parameters obtained by one experimenter using one single apparatus and the same materials against the variability of these parameters among laboratories, and (7) testing the effects of the properties of walls and base of the modeling apparatus by performing the same experiment (with the same material and by the same experimenter) for different materials covering the base and walls.

The results of our benchmark study illustrate the importance for analogue experimental studies of a clear specification of modelling apparatus, set-up technique, material properties and boundary conditions, and may help in establishing the degree to which model results may be extrapolated to natural examples.

C. Beaumont, J.-P. Brun, and B. Colletta are thanked for providing constructive feedback on the design of the experiments, J. Adam and S. Ellis for help in determining the list of parameters to quantify, B. Vendeville for insightful discussions on the importance of boundary conditions and experimental procedures, and the participants of the GeoMod2004 pre-conference workshop for helpful discussions. We also thank J. Adam and B. Vendeville for their encouraging and helpful reviews. This study was supported by Swiss National Science Foundation Grant 2000-067952.02 (GS), the Natural Sciences and Engineering Research Council of Canada (ARC), Deutsche Forschungsgemeinschaft as part of SFB 267 (NK), and the Swedish Research Council, VR (HAK and FN).

References

- ADAM, J., URAI, J. L. *ET AL.* 2005. Shear localization and strain distribution during tectonic faulting – new insights from granular-flow experiments and high-resolution optical image correlation techniques. *Journal of Structural Geology*, **27**, 283–301.
- ATMAOUI, N., KUKOWSKI, N., STÖCKHERT, B. & KÖNIG, D. 2005. Initiation and development of pull-apart basins with riedel shear mechanism: Insights from clay scaled experiments. *International Journal of Earth Sciences*. In press.
- BAHROUDI, A., KOYI, H. A. & TALBOT, C. J. 2003. Effect of ductile and frictional décollements on

- style of extension. *Journal of Structural Geology*, **25**, 1401–1423.
- BARNHOORN, A. BYSTRICKY, M., BURLINI, L. & KUNZE, K. 2004. The role of recrystallization on the deformation behaviour of calcite rocks: large strain torsion experiments on Carrara marble. *Journal of Structural Geology*, **26**, 885–903.
- BRUN, J.-P. 1999. Narrow rifts versus wide rifts: inferences for the mechanics of rifting from laboratory experiments. *Philosophical Transactions, Royal Society London A*, **357**, 695–712.
- BRUN, J.-P., SOKOUTIS, D. & VAN DEN DRIESSCHE, J. 1994. Analogue modelling of detachment fault systems and core complexes. *Geology*, **22**, 319–322.
- BUI TER, S. J. H., BABEYKO, A. YU. ET AL. 2006. The numerical sandbox: Comparison of model results for a shortening and an extension experiment. In: BUI TER, S. J. H. & SCHREURS, G. (eds) *Analogue and Numerical Modelling of Crustal-Scale Processes*. Geological Society, London, Special Publications, **253**, xx–yy.
- BYERLEE, J. 1978. Friction of rocks. *Pure and Applied Geophysics*, **116**, 615–626.
- CADELL, H. M. 1888. Experimental researches in mountain building. *Transactions of the Royal Society of Edinburgh*, **1**, 339–343.
- CASAGRANDE, A. 1932. Research on the Atterberg limits of soils. *Public Roads*, **13**(9), 121–136.
- COLLETTA, B., BALE P., BALLARD, J. F., LETOUZEY, J. & PINEDO, R. 1991. Computerized X-ray tomography analysis of sandbox models: Examples of thin-skinned thrust systems. *Geology*, **19**, 1063–1067.
- COSTA, E., CAMERLENGHI, A. ET AL. 2004. Modelling deformation and salt tectonics in the eastern Mediterranean Ridge accretionary wedge. *Geological Society of America Bulletin*, **116**, 880–894.
- CRUDEN, A. R., NASSERI, M. B. & PYSKLYWEC, R. 2006. Surface topography and internal strain variation in wide hot orogens from three-dimensional analogue and two-dimensional numerical vise models. In: BUI TER, S. J. H. & SCHREURS, G. (eds) *Analogue and Numerical Modelling of Crustal-Scale Processes*. Geological Society, London, Special Publications, **253**, xx–yy.
- DAVIS, D., SUPPE, J. & DAHLEN, F. A. 1983. Mechanics of fold-and-thrust belts and accretionary wedges. *Journal of Geophysical Research*, **88**, B2, 1153–1172.
- ELLIS, S., SCHREURS, G. & PANIEN, M. 2004. Comparisons between analogue and numerical models of thrust wedge development. *Journal of Structural Geology*, **26**, 1659–1675.
- GARTRELL, A. P. 2001. Crustal rheology and its effect on rift basin styles. In: KOYI, H. A. & MANCKTELOW, N. S. (eds) *Tectonic Modeling: A volume in honor of Hans Ramberg*. Geological Society of America Memoir, **193**, 221–233.
- GUTSCHER, M.-A., KUKOWSKI, N., MALAVIEILLE, J. & LALLEMAND, S. 1996. Cyclical behaviour of thrust wedges: Insights from high basal friction sandbox experiments. *Geology*, **24**, 135–138.
- GUTSCHER, M.-A., KUKOWSKI, N., MALAVIEILLE, J. & LALLEMAND, S. 1998. Material transfer in accretionary wedges from analysis of a systematic series of analog experiments. *Journal of Structural Geology*, **20**, 407–416.
- HOTH, S., ADAM, J., KUKOWSKI, N. & ONCKEN, O. 2005. Influence of erosion on the kinematics of bivergent orogens. Results from scaled sandbox simulations. *GSA Special Volume on Tectonics, Climate and Landscape Evolution*. In press.
- HUBBERT, M. K. 1937. Theory of scale models as applied to the study of geological structures. *Geological Society of America Bulletin*, **48**, 1459–1520.
- HUBBERT, M. K. 1951. Mechanical basis for certain geological structures. *Geological Society America Bulletin*, **62**, 355–372.
- JAEGER, J. C. & COOK, N. G. W. 1979. *Fundamentals of rock mechanics*. John Wiley and Sons, New York, 585pp.
- KEEP, M. & MCCLAY, K. R. 1997. Analogue modelling of multiphase rift systems. *Tectonophysics*, **273**, 239–270.
- KONSTANTINOVSKAIA, E. & MALAVIEILLE, J. 2005. Erosion and exhumation in accretionary orogens: Experimental and geological approaches. *Geochemistry, Geophysics, Geosystems (G³)*, **6**, Q02006, DOI 10.1029/2004GC000794.
- KOYI, H. A. 1995. Mode of internal deformation in sand wedges. *Journal of Structural Geology*, **17**, 293–300.
- KOYI, H. A. 1997. Analogue modelling: From a qualitative to a quantitative technique, a historical outline. *Journal of Petroleum Geology*, **20**, 223–238.
- KUKOWSKI, N., LALLEMAND, S. E., MALAVIEILLE, J., GUTSCHER, M.-A. & RESTON, T. J. 2002. Mechanical decoupling and basal duplex formation observed in sandbox experiments with application to the western Mediterranean Ridge accretionary complex. *Marine Geology*, **186**, 29–42.
- LALLEMAND, S. E., SCHNÜRLE, P. & MALAVIEILLE, J. 1994. Coulomb theory applied to accretionary and non-accretionary wedges: Possible causes for tectonic erosion and/or frontal accretion. *Journal of Geophysical Research*, **99**, B6, 12033–12055.
- LOHRMANN, J., KUKOWSKI, N., ADAM, J. & ONCKEN, O. 2003. The impact of analogue material properties on the geometry, kinematics, and dynamics of convergent sand wedges. *Journal of Structural Geology*, **25**, 1691–1771.
- MALAVIEILLE, J. 1984. Modélisation expérimentale des chevauchements imbriqués: application aux chaînes de montagnes. *Bulletin Société Géologique de France*, **7**, 129–138.
- MARONE, C. 1998. Laboratory-derived friction laws and their application to seismic faulting. *Annual Review of Earth and Planetary Sciences*, **26**, 643–696.
- MUGNIER, J. L., BABY, P., COLLETTA, B., VINOUR, B., BALE, P. & LETURMY, P. 1997. Thrust geometry controlled by erosion and sedimentation: A view from analogue models. *Geology*, **25**, 427–430.
- MULUGETA, G. 1988. Modelling the geometry of Coulomb thrust wedges. *Journal of Structural Geology*, **10**, 847–859.

- MULUGETA, G. & KOYI, H. 1987. Three-dimensional geometry and kinematics of experimental piggy-back thrusting. *Geology*, **15**, 1052–1056.
- MULUGETA, G. & KOYI, H. 1992. Episodic accretion and strain partitioning in a model sand wedge. *Tectonophysics*, **202**, 319–322.
- PANIEN, M. 2004. Analogue modelling experiments of basin inversion using well-characterized granular materials and comparisons with numerical models. Ph.D. thesis. University of Bern, Switzerland.
- PANIEN, M., BUITER, S. J. H., SCHREURS, G. & PFIFFNER, O. A. 2006. Inversion of a symmetric basin: Insights from a comparison between analogue and numerical experiments. In: BUITER, S. J. H. & SCHREURS, G. (eds) *Analogue and Numerical Modelling of Crustal-Scale Processes*. Geological Society, London, Special Publications, **253**, xx–yy.
- PYSKLYWEC, R. N. & CRUDEN, A. R. 2004. Coupled crust-mantle dynamics and intraplate tectonics: two-dimensional numerical and three-dimensional analogue modelling. *Geochemistry, Geophysics Geosystems G³*, **5**(10), DOI 10.1029/2004GC000748.
- RAMBERG, H. 1981. *Gravity, deformation and the Earth's crust*. Academic Press, London.
- SCHELLART, W. P. 2000. Shear test results for cohesion and friction coefficients for different granular materials: scaling implications for their usage in analogue modelling. *Tectonophysics*, **324**, 1–16.
- SCHREURS, G., HÄNNI, R. & VOCK, P. 2001. Four-dimensional analysis of analog models: Experiments on transfer zones in fold and thrust belts. In: KOYI, H. A. & MANCKTELOW, N. S. (eds) *Tectonic Modeling: A volume in honor of Hans Ramberg*. Geological Society of America Memoir, **193**, 179–190.
- SCHULZE, D. 1994. Entwicklung und Anwendung eines neuartigen Ringschergerätes. *Aufbereitungstechnik*, **35**(10), 524–535.
- SIMS, D. 1993. The rheology of clay: a modeling material for geologic structures: *EOS, Transactions, American Geophysical Union*, **74**, 569.
- STORTI, F. & McCLAY, K. 1995. Influence of syntectonic sedimentation on thrust wedges in analogue models. *Geology*, **23**, 999–1002.
- STORTI, F., SALVINI, F. & McCLAY, K. 2000. Synchronous and velocity-partitioned thrusting and thrust polarity reversal in experimentally produced doubly-vergent thrust wedges: Implications for natural orogens. *Tectonics*, **19**(2), 378–396.
- TEN GROTENHUIS, S. M., PIAZOLO, S., PAKULA, T., PASSCHIER, C. W. & BONIS, P.D. 2002. Are polymers suitable rock analogs? *Tectonophysics*, **350**, 35–47.
- TRON, V. & BRUN, J-P. 1991. Experiments on oblique rifting in brittle-ductile systems. *Tectonophysics*, **188**, 71–84.
- TURRINI, C., RAVAGLIA, A. & PEROTTI, C. 2001. Compressional structures in a multilayered mechanical stratigraphy: Insights from sandbox modeling with three-dimensional variations in basal geometry and friction. In: KOYI, H. A. & MANCKTELOW, N. S. (eds) *Tectonic Modeling: A volume in honor of Hans Ramberg*. Geological Society of America Memoir, **193**, 158–178.
- VENDEVILLE, B. C. 1987. *Champs de failles et tectonique en extension: modélisation expérimentale*. Ph.D. thesis University of Rennes I, 392pp.
- VENDEVILLE, B. C. & JACKSON, M. P. A. 1992a. The rise of diapirs during thin-skinned extension. *Marine Petroleum Geology*, **9**, 331–353.
- VENDEVILLE, B. C. & JACKSON, M. P. A. 1992b. The fall of diapirs during thin-skinned extension. *Marine Petroleum Geology*, **9**, 354–371.
- WEIJERMARS, R. 1986. Flow behaviour and physical chemistry of bouncing putties and related polymers in view of tectonic laboratory applications. *Tectonophysics*, **124**, 325–358.
- WITHJACK, M. O. & CALLAWAY, S. 2000. Active normal faulting beneath a salt layer; an experimental study of deformation patterns in the cover sequence. *AAPG Bulletin*, **84**, 627–651.

